EuroSun2026

RECONSTRUCTING GLOBAL HORIZONTAL SOLAR SPECTRA FROM DIRECT SPECTRAL MEASUREMENTS THROUGH ATMOSPHERIC PARAMETER RETRIEVAL

Gabriel López[1] (corresponding author), Rodrigo Álvarez-Barajas[2], M. Pilar Orihuela[1], Enrique García[3], Joaquín Alonso-Montesinos[3], Jesús Polo[4] and Jesús Ballestrín[5]

[1] *Dpto. Ingeniería Eléctrica y Térmica, de Diseño y Proyectos, Universidad de Huelva (Spain)*
[2] *Solar Consulting Services, (USA)*
[3] *Dpto. Química y Física, Universidad de Almería (Spain)*
[4] *Unidad de Energía Solar Fotovoltaica, CIEMAT (Spain)*
[5] *CIEMAT-Plataforma Solar de Almería. Point Focus Solar Thermal Technologies Unit (Spain)*

gabriel.lopez@die.uhu.es

Summary

This study presents a methodology to estimate the global horizontal solar spectrum over the 280–4 000 nm range using atmospheric parameters retrieved from spectral direct normal irradiance (DNI) measurements through a Genetic Algorithm (GA) coupled with a Radiative Transfer Model (RTM). The retrieved atmospheric parameters are used as inputs to the SMARTS RTM to reconstruct the global spectral irradiance. The reconstruction is validated against independent spectroradiometric measurements over the 294–1 100 nm range and against broadband pyranometer measurements over 285–3 000 nm. Results show very good agreement within the measured spectral range and high consistency in integrated broadband irradiance when compared with pyranometer measurements. The RTM-GA framework therefore provides a physically consistent basis for estimating global spectral irradiance from retrieved atmospheric parameters. The proposed methodology enables the generation of full shortwave solar spectra beyond the instrumental limits of conventional spectroradiometers while simultaneously providing a diagnostic reference for instrument performance assessment under real operating conditions.

Keywords: GHI spectra, DNI spectra, SMARTS, photovoltaic

Field of application for the findings: precise performance modeling and spectral optimization in advanced photovoltaic and agrivoltaic systems

Addressed audience: photovoltaic research community

1. Introduction

Solar radiation reaching the Earth's surface exhibits continuous variations in its spectral distribution due to scattering and absorption processes by atmospheric constituents. These phenomena cause substantial departures from standard reference spectra and can lead to markedly different spectral distributions under similar broadband irradiance conditions. Understanding this spectral variability is critical for technologies with wavelength-dependent conversion mechanisms, such as selective solar thermal collectors, agrivoltaics, and photovoltaics (PV) (Stanley et al., 2016). In PV systems, the spectral response varies significantly across semiconductor materials, causing technology-dependent energy gains and losses that may reach several percentage points on an annual basis relative to standard reference conditions (Conde et al., 2021; Kinsey et al., 2022). Consequently, access to realistic spectral information is crucial for accurate solar resource assessment and advanced performance modeling.

Despite its relevance, continuous measurements of solar spectral irradiance remain scarce worldwide, as spectroradiometric measurements require relatively complex and expensive instrumentation, together with regular calibration and careful maintenance (Paraskeva et al., 2014). This limitation has driven the development of alternative estimation methods, including semi-empirical formulations, satellite products, and radiative transfer models (RTMs) (Lindsay et al., 2020). These numerical models allow the simulation of spectral irradiance from key atmospheric parameters such as aerosol optical depth (AOD), Ångström exponent (AE), precipitable water vapour (PW), and ozone content (Xue et al., 2015; Khakhu et al., 2023).

Coupling heuristic optimization techniques such as genetic algorithms (GAs) with RTMs has emerged as an effective strategy for retrieving atmospheric properties directly from solar measurements. For example, a GA coupled with the SMARTS model (Gueymard, 2019) was successfully used to infer AOD at 500 nm (AOD_{500}), AE, and PW from measured direct normal irradiance (DNI) spectra, enabling accurate reconstruction and spectral extension of the direct beam (López et al., 2026).

While previous studies have primarily focused on atmospheric parameter retrieval or DNI spectral reconstruction, comparatively little attention has been paid to generating complete global horizontal irradiance (GHI) spectra from DNI observations through atmospheric parameter retrieval. Since spectral DNI measurements have traditionally been used for atmospheric characterization and radiative transfer studies, the ability to derive spectrally resolved GHI from the retrieved atmospheric state considerably extends the value of these observations. Moreover, it constitutes an essential intermediate step towards estimating spectrally resolved irradiance on tilted planes for advanced PV yield and microclimate assessments.

To address this gap, the objective of this work is to evaluate the feasibility and accuracy of reconstructing GHI spectra over the 280–4 000 nm range from measured spectral DNI using the RTM-GA optimization framework. The reconstruction is validated against independent high-resolution spectroradiometric measurements over 294–1 100 nm and against broadband pyranometric measurements over 285–3 000 nm, collected under contrasting atmospheric conditions in southwestern Spain, establishing a robust tool for advanced solar energy applications.

2. Experimental setup

Measurements were conducted at the Solar Testing Laboratory of the Universidad de Huelva (Fig. 1), located at the La Rábida Campus in southwestern Spain (37.2°N, 6.92°W). Spectral solar irradiance has been routinely monitored since February 2021 as part of experimental research programmes devoted to atmospheric characterization and spectral solar resource assessment. Spectral DNI was measured using an EKO MS-700N spectroradiometer covering the 350–1 050 nm wavelength range, while spectral GHI, G_λ, was monitored using an EKO MS-711 spectroradiometer operating between 294 and 1 100 nm. In parallel, broadband GHI, G, and diffuse horizontal irradiance (DHI) were continuously recorded by secondary-standard EKO MS-802 pyranometers with spectral sensitivity extending from 285 to 3 000 nm. Spectral measurements obtained with the MS-700N and MS-711 spectroradiometers correspond to instantaneous spectra acquired every minute. Broadband irradiance data from the MS-802 pyranometers were recorded as one-minute averages derived from irradiance measurements sampled at 1 s intervals during the corresponding averaging period. The experimental data are supplemented with one-minute atmospheric temperature, relative humidity, and pressure measurements recorded with a WD-500 sensor (Lufft GmbH, Fellbach, Germany).

The present study focuses on cloud-free conditions in order to isolate the influence of atmospheric constituents on the spectral distribution of solar irradiance. Two representative days were selected for detailed analysis. The first one, March 24, 2021, corresponds to exceptionally clean atmospheric conditions characterized by very low aerosol loading and high atmospheric transparency. The second one, April 4, 2021, was affected by a Saharan dust intrusion producing significantly increased AOD and noticeable spectral attenuation. These two days provide contrasting atmospheric scenarios that facilitate the evaluation of the proposed reconstruction methodology.

To assess the robustness of the approach, five additional cloud-free days covering a broad range of atmospheric conditions representative of southwestern Spain were included in the validation dataset, as summarized in Table 1. These cases span from pristine conditions to intense Saharan dust events, with AOD_{500} values up to 1.62 and PW varying from 1.2 to 3.1 cm. In total, 2 241 spectral DNI measurements were processed across the seven cloud-free validation days for atmospheric parameter retrieval.

These retrieved atmospheric parameters were subsequently used to reconstruct GHI spectra. Spectroradiometric GHI measurements from the MS-711 were available for six of the seven validation days; MS-711 measurements were not available on July 11, 2021. Consequently, spectral validation was performed using the six days for which

Fig. 1: Solar Testing Laboratory of the Universidad de Huelva (Spain).

Tab. 1: Summary of the cloud-free validation cases, including the dominant atmospheric conditions, analysed time intervals, interval-averaged retrieved values of AOD_{500}, AE and PW, and the corresponding number N of spectral DNI observations used for atmospheric parameter retrieval.

Date	Atmospheric condition	Hourly interval (UT)	AOD_{500}	AE	PW (cm)	N
2021-03-24	Pristine atmosphere	10:44-17:30	0.1	1.9	1.2	407
2021-04-04	Saharan dust event	06:30-14:29	0.3	0.85	2.4	480
2021-05-04	Low aerosol loading	08:20-09:20	0.15	1.5	2.5	60
2021-05-06	Clean atmosphere	07:30-13:30	0.1	2.3	1.8	361
2021-06-08	Dust intrusion onset	08:00-12:00	0.11	1.8	2.5	241
2021-06-10	Dust outbreak peak	09:00-13:30	0.3	0.8	3.0	331
2021-07-11	Extreme aerosol event	08:00-14:00	1.62	0.1	3.1	361

independent GHI spectra were available. Broadband pyranometric measurements, however, were available for all seven validation days and were therefore used to assess the consistency of the reconstructed broadband GHI over the complete validation dataset. The broadband validation was based on comparisons between the measured GHI from the MS-802 pyranometer and the GHI obtained by integrating the reconstructed RTM-GA spectra over the corresponding broadband spectral range.

3. Methodology

The atmospheric conditions relevant to the present reconstruction are characterized by three key parameters: AOD_{500}, AE, and PW, which are obtained using the RTM-GA approach developed by López et al. (2026). In this methodology, the SMARTS RTM is coupled with a GA that iteratively searches for the combination of these three atmospheric parameters that minimizes the difference between measured and simulated DNI spectra under cloud-free conditions.

The retrieved atmospheric parameters are subsequently used as inputs to SMARTS to generate GHI spectra. Unlike the application reported by López et al. (2026), which focused on DNI spectral reconstruction and extension beyond the instrument spectral range, the present study employs the retrieved atmospheric parameters to reconstruct spectral GHI over the 280–4 000 nm wavelength range.

Since SMARTS produces spectra at a much higher spectral resolution than the EKO MS-711 spectroradiometer, simulated spectra must be adapted before comparison with measurements. This is achieved through a wavelength-dependent Gaussian convolution that projects the SMARTS output onto the MS-711 wavelength grid. In the absence of detailed slit-function information from the manufacturer, the instrument response is reasonably approximated by a Gaussian function with a full width at half maximum (FWHM) of 7 nm.

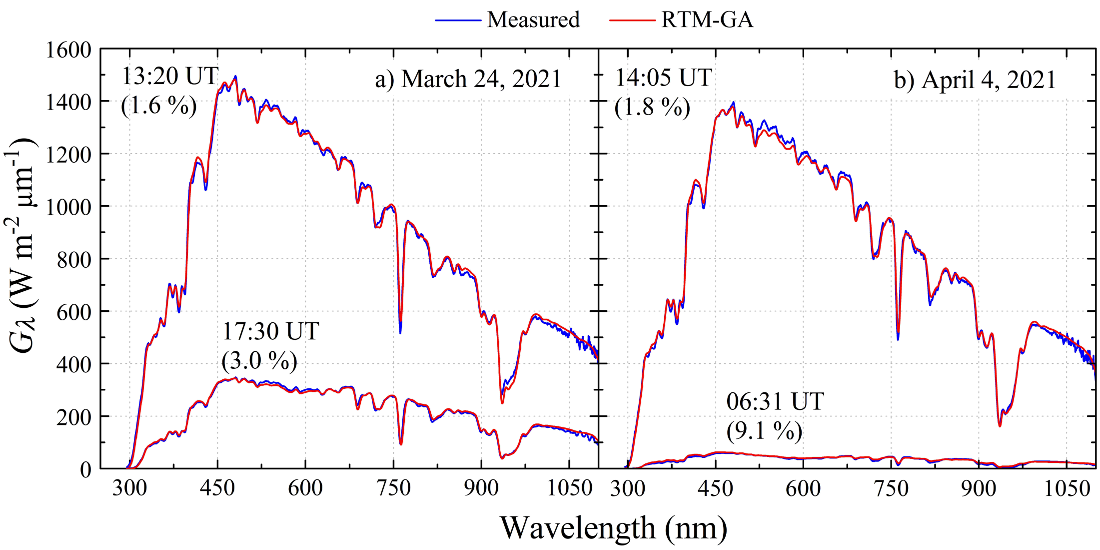

Fig. 2: Measured and RTM-GA reconstructed GHI spectra for representative cloud-free conditions corresponding to (a) a pristine atmosphere (March 24, 2021) and (b) a Saharan dust event (April 4, 2021). The values of the spectral error function J are indicated for each spectrum.

4. Results

The reconstructed GHI spectra $G_{\lambda,\mathrm{RTM-GA}}$ are compared with the observed spectra $G_{\lambda,\mathrm{obs}}$ over the common wavelength range from $\lambda_1 = 294$ nm to $\lambda_2 = 1\,100$ nm and integrated to obtain broadband irradiance values. Spectral agreement is evaluated using the error function J:

$$J(\%) = 100 \times \frac{\sqrt{\int_{\lambda_1}^{\lambda_2} (G_{\lambda,\mathrm{RTM-GA}} - G_{\lambda,\mathrm{obs}})^2 \, \mathrm{d}\lambda}}{\sqrt{\int_{\lambda_1}^{\lambda_2} G_{\lambda,\mathrm{obs}}^2 \, \mathrm{d}\lambda}}, \tag{1}$$

where the normalization by the measured spectrum makes J independent of the absolute irradiance level. The resulting metric provides a convenient percentage measure of the overall spectral agreement between reconstructed and observed spectra. Broadband agreement is subsequently evaluated using standard statistical indicators—RMSE, MBE, and the coefficient of determination (R^2)—with RMSE and MBE expressed as percentages of the mean measured irradiance.

Figure 2 compares measured and reconstructed GHI spectra for two representative cloud-free days corresponding to a pristine atmosphere (March 24, 2021) and a Saharan dust event (April 4, 2021). For each day, two spectra were selected to illustrate different levels of reconstruction performance. For March 24, the spectra corresponding to the minimum (J = 1.6 %) and maximum (J = 3.0 %) error values obtained during the analysed interval are shown. For April 4, the selected spectra correspond to the minimum (J = 1.8 %) and maximum (J = 9.1 %) error values obtained during the analysed interval. Excellent agreement is observed across the measured spectral range in all cases. The reconstructed spectra reproduce the overall spectral shape and the main atmospheric absorption features within the experimentally validated spectral range, even under the least favourable conditions.

The similarity of the minimum J values obtained under clean and dust-laden conditions indicates that high spectral agreement can be achieved under substantially different aerosol loads. The largest discrepancy shown in Fig. 2 corresponds to the early-morning spectrum of April 4, 2021 (J = 9.1 %), while the March 24 afternoon case (J = 3.0 %) illustrates the good performance achieved even at comparatively large solar zenith angles. Despite the larger discrepancies observed in these situations, the reconstructed spectra still capture the dominant spectral features, the main atmospheric absorption bands, and the overall spectral energy distribution.

Above approximately 1 000 nm, the measured spectra exhibit oscillations that are not consistent with the expected smooth behaviour of cloud-free solar irradiance. These fluctuations are likely associated with instrumental noise and the reduced signal-to-noise ratio of the MS-711 spectroradiometer in the near-infrared region. In

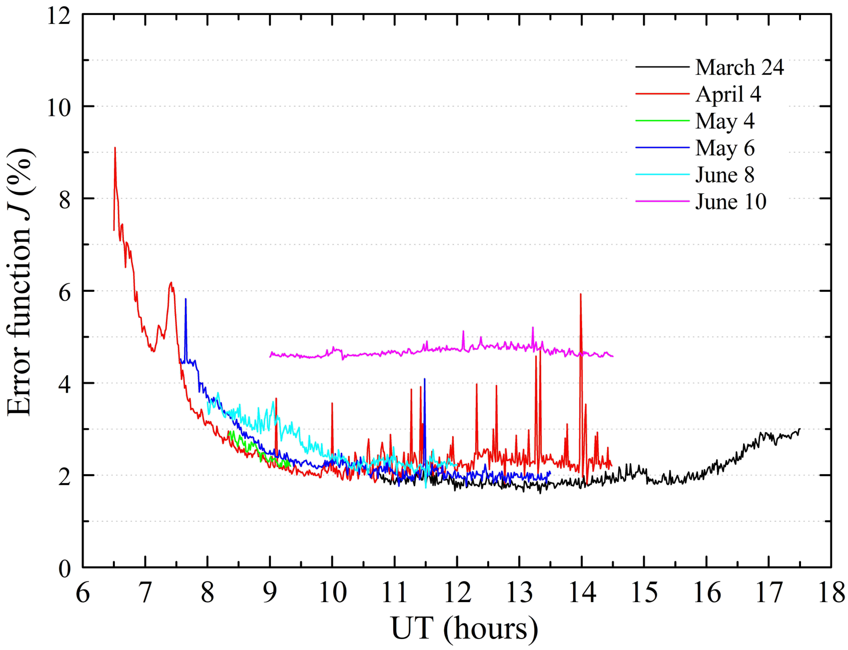

Fig. 3: Temporal evolution of the spectral error function J for the six cloud-free validation days considered in this study.

contrast, the RTM-GA reconstruction provides a physically consistent spectral profile, highlighting the potential of the methodology as a complementary tool for spectral quality control.

Figure 3 presents the temporal evolution of the spectral error function J for the six validation days for which independent GHI spectral measurements were available. For March 24, May 4, May 6, and June 8, error values generally remain below 4 %, reaching minima close to 2 % during large portions of the analysed intervals. Similar behaviour is obtained for April 4, although larger discrepancies appear shortly after sunrise when both measurements and simulations become more sensitive to uncertainty sources associated with large solar zenith angles and low irradiance levels.

The largest sustained discrepancies are observed on June 10, corresponding to the peak of a Saharan dust outbreak. In this case, J remains relatively stable throughout most of the analysed period, with values around 4.5–5%, which are only moderately higher than those obtained under cleaner atmospheric conditions. Since the RTM-GA methodology was previously shown to accurately reproduce the measured DNI spectra under all analysed conditions (López et al., 2026), these differences cannot be attributed solely to the retrieval of AOD_{500}, AE, and PW. Furthermore, similarly good agreement obtained on April 4 under comparable aerosol conditions suggests that atmospheric turbidity alone is not sufficient to explain the observed discrepancies. A preliminary analysis indicates that the remaining differences are mainly associated with the diffuse contribution to GHI, whose relative importance increases under dusty atmospheric conditions. Additional factors not fully characterized by the retrieved atmospheric parameters may also contribute to these differences. A detailed assessment of the relative contribution of each factor falls beyond the scope of the present work and deserves further investigation.

Figure 4 illustrates one of the principal advantages of the proposed methodology. The figure presents the extended and upscaled RTM-GA spectral reconstruction for two representative cases. The first corresponds to the best agreement obtained under the pristine atmospheric conditions of March 24, 2021 (J = 1.6 %), previously shown in Fig. 2. The second corresponds to April 4, 2021, under Saharan dust conditions. The spectrum displayed for April 4 was selected 30 minutes after the highest-error spectrum shown in Fig. 2 (J = 9.1 % at 06:31 UT), since the higher irradiance level at 07:00 UT allows a clearer representation of the extended spectral distribution while preserving similar atmospheric conditions.

While the MS-711 spectroradiometer is limited to the 294–1 100 nm range and measures at its instrumental spectral resolution, the extended and upscaled RTM-GA reconstruction provides continuous high-resolution spectra over the entire shortwave domain simulated by SMARTS. For visualization purposes, only the interval up to 2 500 nm is shown, although the simulations extend to 4 000 nm. The reconstructed spectra reveal significant

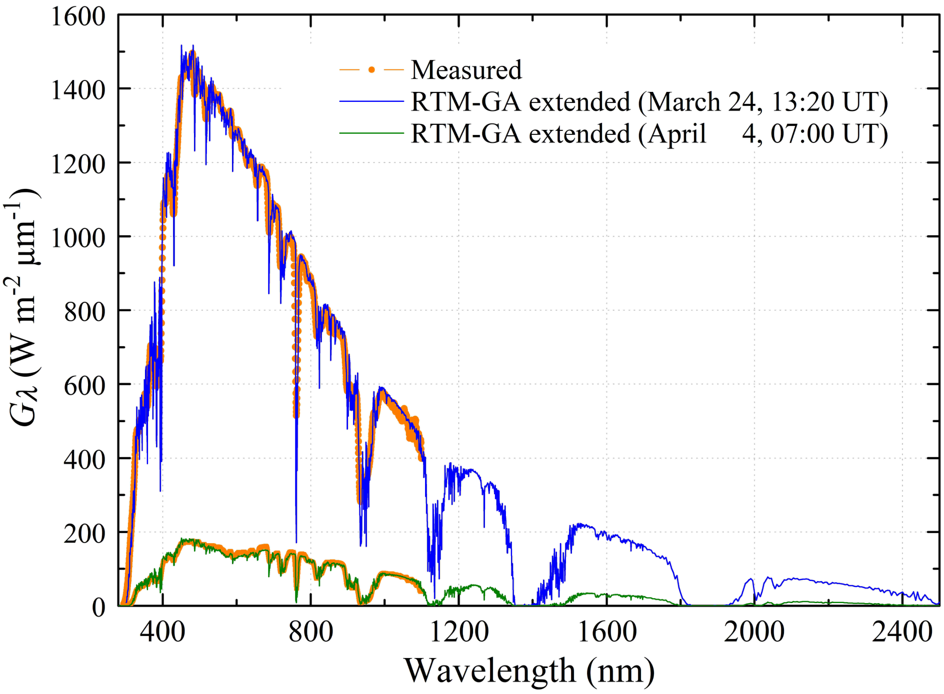

Fig. 4: Measured GHI spectra and corresponding RTM-GA extended and upscaled reconstructions for representative cases on March 24 and April 4, 2021. The methodology reproduces the measured spectra within the MS-711 spectral range and simultaneously provides high-resolution spectral irradiance beyond the instrumental limits. For clarity, only the wavelength range up to 2 500 nm is shown, although SMARTS simulations extend to 4 000 nm.

irradiance contributions beyond the instrumental limits, together with detailed near-infrared absorption features associated with atmospheric water vapour.

This capability is especially relevant because broadband irradiance depends on wavelengths well beyond those measured by the spectroradiometer. Consequently, broadband GHI cannot in general be uniquely determined from measurements restricted to the 294–1 100 nm interval, since different atmospheric states may produce similar spectral distributions within the measured range while yielding different irradiance contributions at longer wavelengths. By reconstructing the complete spectral distribution, the RTM-GA methodology enables physically consistent broadband irradiance estimates while preserving agreement with the measured spectra.

Figure 5 compares the daily evolution of broadband GHI from pyranometer measurements, extended and upscaled RTM-GA spectra integrated over 285–3 000 nm, and both measured and reconstructed spectra integrated over the spectroradiometer range (294–1 100 nm). Within the MS-711 spectral interval, excellent agreement is obtained for all six validation days for which independent GHI spectral measurements were available, as confirmed by the statistics reported in Table 2. Values of R^2 range from 0.95 to 0.99, while RMSE remains below 2.3 % of the mean irradiance. The associated MBE values are also small, ranging from −2.1 % to 1.5 %, indicating the absence of significant systematic bias. These results demonstrate that the RTM-GA methodology accurately reproduces the integrated GHI within the measured spectral range under both pristine and aerosol-laden atmospheric conditions, including the peak of the Saharan dust outbreak on June 10, 2021.

A more demanding validation is obtained by comparing broadband irradiance derived from the extended and upscaled reconstructed spectra against pyranometer measurements. Excellent agreement is achieved for all validation days except July 11, with R^2 = 0.99 in the broadband comparison for both pristine and aerosol-laden conditions. A marked deterioration in the broadband agreement is observed under the most extreme aerosol conditions, reaching RMSE = 16.6 %, MBE = −15.3 %, and R^2 = 0.65 during the extreme aerosol event of July 11. This behaviour is consistent with the observations discussed previously for the spectral validation, where part of the remaining discrepancies were associated with the diffuse contribution to GHI. Under the exceptionally high aerosol loading conditions of July 11, the relative contribution of diffuse irradiance is expected to increase further, which may contribute to the deterioration of the broadband reconstruction. Despite these discrepancies, the methodology reproduces broadband irradiance with good overall consistency across a

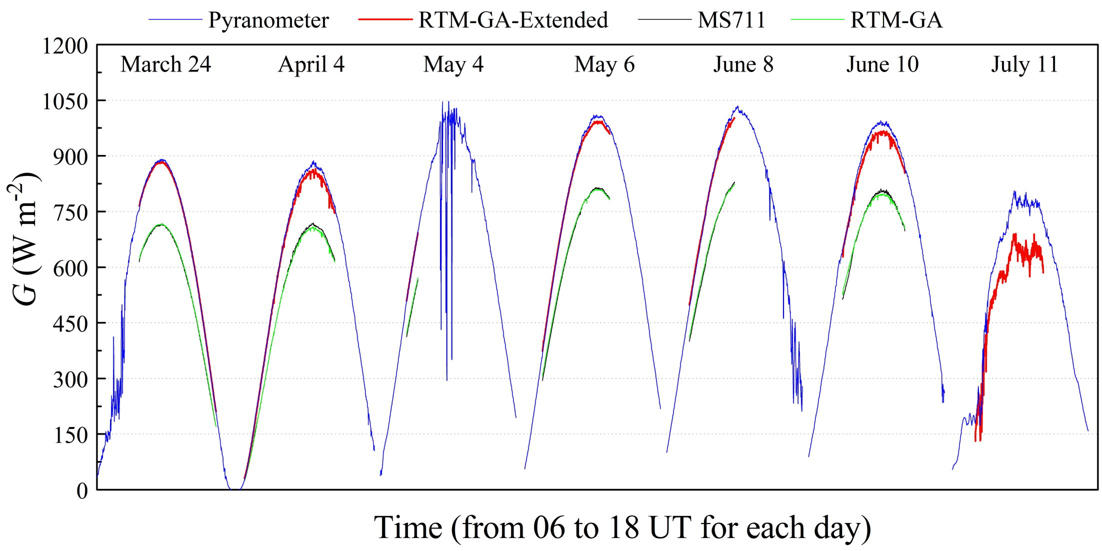

Fig. 5: Daily evolution of broadband GHI for the seven validation days. Blue curves represent pyranometer measurements (MS-802), red curves correspond to RTM-GA reconstructed spectra integrated over the extended spectral range (285–3 000 nm), and black and green curves correspond to measured and reconstructed spectra integrated over the MS-711 spectral range (294–1 100 nm), respectively. MS-711 measurements were not available on July 11, 2021.

wide range of atmospheric conditions and demonstrates the feasibility of generating physically consistent GHI spectra beyond the instrumental limits of conventional spectroradiometers.

Tab. 2: Statistical comparison of integrated GHI spectra. The left columns show the statistical comparison between broadband pyranometer measurements (285–3 000 nm) and the extended and upscaled RTM-GA reconstructions, while the right columns show the corresponding comparison between measured and reconstructed GHI spectra integrated over the MS-711 spectral range (294–1 100 nm). RMSE and MBE values correspond to the percentage relative to the mean measured value.

	Broadband Pyranometric GHI			**Measured & Reconstructed Spectra**		
Date	R^2	**RMSE (%)**	**MBE (%)**	R^2	**RMSE (%)**	**MBE (%)**
2021-03-24	0.99	0.6	−0.2	0.99	0.6	0.6
2021-04-04	0.99	2.1	−1.6	0.99	1.2	−0.8
2021-05-04	0.99	0.3	0.0	0.97	1.5	1.5
2021-05-06	0.99	1.3	−0.6	0.99	1.1	0.6
2021-06-08	0.99	1.4	−0.5	0.99	1.1	0.8
2021-06-10	0.99	1.4	0.0	0.95	2.2	−2.1
2021-07-11	0.65	16.6	−15.3	–	–	–

5. Conclusions

A methodology for reconstructing global horizontal spectral irradiance from measured direct normal spectral irradiance has been presented and experimentally validated. Atmospheric parameters retrieved from DNI spectra using the RTM-GA framework (AOD_{500}, AE, and PW) were successfully employed as inputs to the SMARTS radiative transfer model to generate physically consistent GHI spectra. Validation against independent GHI spectral measurements demonstrated excellent agreement within the spectral range covered by the MS-711 spectroradiometer (294–1 100 nm). For the validation days with available spectroradiometric GHI measurements, the spectral error function J generally remained below 5 %, reaching minimum values close to 2 % under both pristine and dust-laden conditions. Broadband validation further confirmed the consistency of the reconstructed spectra, with coefficients of determination close to unity and percentage RMSE values generally below 2 % for all validation days except July 11.

Beyond reproducing the measured spectral range, the proposed methodology provides physically consistent high-resolution spectra over the full shortwave domain simulated by SMARTS. This capability enables broadband irradiance estimation from limited spectral observations and may also facilitate the identification of spectral inconsistencies and instrumental artefacts. The larger discrepancies observed during the extreme aerosol event of July 11 could not be explained solely by the retrieved atmospheric parameters or by aerosol loading itself, particularly considering the excellent agreement obtained during the Saharan dust outbreak peak on June 10. The results suggest that additional processes affecting the diffuse contribution to GHI become increasingly relevant under highly turbid atmospheric conditions and deserve further investigation.

Overall, the results demonstrate that atmospheric information extracted from spectral DNI measurements can be successfully transferred to reconstruct spectral GHI. The methodology therefore represents a practical pathway towards generating extended and upscaled spectral irradiance datasets from limited measurements and constitutes an important step towards future applications involving plane-of-array spectral irradiance, advanced photovoltaic modelling, agrivoltaic systems, and other solar-energy technologies requiring spectrally resolved solar resource characterization.

Acknowledgements

This work has been supported by the Spanish Ministerio de Ciencia, Innovación y Universidades (MICIU/AEI/10.13039/501100011033) and co-funded by the European Union (FEDER) through the coordinated project CARSOLAND (Refs. PID2025-171444OB-C31, -C32, and -C33).

References

L.A. Conde, J.R. Angulo, M.A. Sevillano-Bendezú, G. Nofuentes, J.A. Töfflinger, and J. de la Casa. Spectral effects on the energy yield of various photovoltaic technologies in Lima (Perú). *Energy*, 223:120034, 2021. ISSN 0360-5442. doi: 10.1016/j.energy.2021.120034.

C.A. Gueymard. The SMARTS spectral irradiance model after 25 years: New developments and validation of reference spectra. *Solar Energy*, 187:233–253, 2019. doi: 10.1016/j.solener.2019.05.048.

S. Khakhu, I. Masiri, R. Wattan, and S. Janjai. A model for the estimation of global spectral solar irradiance under all-sky conditions for Nakhon Pathom station, Thailand. *Journal of Physics: Conference Series*, 2431 (1):012007, 2023. doi: 10.1088/1742-6596/2431/1/012007.

G.S. Kinsey, N.C. Riedel-Lyngskær, A.A. Miguel, M. Boyd, M. Braga, C. Shou, R.R. Cordero, B.C. Duck, C.J. Fell, S. Feron, G.E. Georghiou, N. Habryl, J.J. John, N. Ketjoy, G. López, A. Louwen, E.L. Maweza, T. Minemoto, A. Mittal, C. Molto, G. Neves, G.N. Garrido, M. Norton, B.R. Paudyal, E.B. Pereira, Y. Poissant, L. Pratt, Q. Shen, T. Reindl, M. Rennhofer, C.D. Rodríguez-Gallegos, R. Rüther, W. van Sark, M.A. Sevillano-Bendezú, H. Seigneur, J.A. Tejero, M. Theristis, J.A. Töfflinger, C. Ulbrich, W.A. Vilela, X. Xia, and M.A. Yamasoe. Impact of measured spectrum variation on solar photovoltaic efficiencies worldwide. *Renewable Energy*, 196:995–1016, 2022. doi: 10.1016/j.renene.2022.07.011.

N. Lindsay, Q. Libois, J. Badosa, A. Migan-Dubois, and V. Bourdin. Errors in PV power modelling due to the lack of spectral and angular details of solar irradiance inputs. *Solar Energy*, 197:266–278, 2020. doi: 10.1016/j.solener.2019.12.042.

G. López, B. Ivorra, P. Ferrada, and C.A. Gueymard. An efficient genetic algorithm method to extend and upscale direct solar irradiance spectra measured with spectroradiometers. *Solar Energy*, 305:114242, 2026. doi: 10.1016/j.solener.2025.114242.

V. Paraskeva, M. Norton, H. Maria, and G. Georghiou. *Calibration of Spectroradiometers for Outdoor Direct Solar Spectral Irradiance Measurements*. 2014. ISBN 3-936338-33-7. doi: 10.4229/28thEUPVSEC2013-4AV.6.35.

C. Stanley, A. Mojiri, and G. Rosengarten. Spectral light management for solar energy conversion systems. *Nanophotonics*, 5(1):161–179, 2016. doi: 10.1515/nanoph-2016-0035.

Y. Xue, J. Hashimoto, and K. Otani. Solar spectrum estimation and impact of input parameters. *Journal of the Japan Institute of Energy*, 94(10):1148–1153, 2015. doi: 10.3775/jie.94.1148.